

# HORIZONTAL CONVECTIVE BOILING OF R134A, R1234YF/R134A, AND R1234ZE(E) WITHIN A MICRO-FIN TUBE

M. A. Kedzierski<sup>1,\*</sup> & K.-J. Park<sup>2</sup>

<sup>1</sup>National Institute of Standards and Technology, Gaithersburg, Maryland 20899, USA

<sup>2</sup>Korea Atomic Energy Research Institute, 989-111 Daedeok-daero, Yuseong-gu, Daejeon, 305-353, Korea

\*Address all correspondence to M. A. Kedzierski E-mail: Mark.Kedzierski@NIST.GOV

*This paper presents local convective boiling measurements in a micro-fin tube for R134a and two low global warming potential (GWP) refrigerants: R1234yf/R134a (56/44% mass) and R1234ze(E). The heat-transfer coefficients of the three test fluids were compared at the same heat flux, saturated refrigerant temperature, and refrigerant mass flux using an existing correlation from the literature. The resulting comparison showed that refrigerant R134a exhibited the highest heat-transfer performance in large part due to its higher thermal conductivity compared to the tested low-GWP refrigerants. For the example case presented here, the heat-transfer coefficient for R1234yf/R134a (56/44) remained within 5% of the heat-transfer coefficient for R134a, having essentially identical performance for qualities less than 30%. The heat-transfer coefficient for R1234ze(E) is roughly  $700 \text{ kW/K}^{-1} \cdot \text{m}^{-2}$  (approximately 14%) less than that of R134a for qualities greater than 30%. The smaller heat-transfer coefficient of R1234ze(E) compared to that of R134a is primarily due to the 11% smaller thermal conductivity and the 21% smaller reduced pressure compared to R134a at this test temperature.*

**KEY WORDS:** *flow boiling, extended surface, enhanced heat transfer, low-GWP refrigerant, refrigerant mixtures*

## 1. INTRODUCTION

Internally enhanced tubes, such as micro-fin tubes, are used by most manufacturers in the construction of evaporators and condensers for new unitary refrigeration and air-conditioning equipment. The reason for the micro-fin tube's hold on unitary equipment is that it provides the highest heat transfer with the lowest pressure drop in commercially available internal enhancements (Webb and Kim, 2005). Most of the experimental measurements for evaporative heat-transfer coefficients in micro-fin tubes have been done for traditional refrigerants such as R134a. Pressure from the policies set by the Montreal Protocol (1987), Kyoto Protocol (1997) and European Mobile Directive (2006) have caused a recent shift to refrigerants with both zero ozone depletion potential (ODP) and low global warming potential (GWP). Johnson et al. (2012)

reported that azeotropic R1234yf/R134a (56/44) (i.e., XP10)<sup>1</sup> and R1234ze(E) are among the low-GWP refrigerants identified for evaluation by the Air-Conditioning, Heating, and Refrigeration Institute (AHRI) Low-GWP Alternative Refrigerants Evaluation Program as potential replacement refrigerants for R134a. The reason for this is that both R1234yf/R134a (56/44) and R1234ze(E) have zero ODP and 100 year GWPs [Intergovernmental Panel on Climate Change (IPCC), 2007] of approximately 600 and 6, respectively (Hickman, 2012; Bitzer Kuhlmaschi-

<sup>1</sup>Certain trade names and company products are mentioned in the text or identified in an illustration in order to adequately specify the experimental procedure and equipment used. In no case does such an identification imply recommendation or endorsement by the National Institute of Standards and Technology (NIST), nor does it imply that the products are necessarily the best available for the purpose.

### NOMENCLATURE

$A_c$	cross-sectional area	$T$	temperature (K)
$Bo$	Local boiling number ( $q''/G_r i_{fg}$ )	$t_w$	tube wall thickness (mm)
$C$	coefficients given in Eq. (5)	$U$	expanded relative uncertainty
$c_p$	specific heat (J/kg · K)	$x_q$	thermodynamic mass quality
$D_e$	equivalent inner diameter of smooth tube, $\sqrt{4/A_c\pi}$ (m)	$z$	axial distance (m)
$D_h$	hydraulic diameter of micro-fin tube (m)	<b>Greek Symbols</b>	
$e$	fin height (mm)	$\alpha$	helix angle ( $^\circ$ )
$G$	total mass velocity (kg/m <sup>2</sup> · s)	$\beta$	fin angle ( $^\circ$ )
$h_{2\phi}$	local two-phase heat-transfer coefficient (W/m <sup>2</sup> · K)	$\Delta T_s$	$T_s - T_w$ (K)
$i_{fg}$	latent heat of vaporization (J/kg)	$\mu$	viscosity (Pa · s)
$k$	refrigerant thermal conductivity (W/m · K)	$v$	specific volume [ $x_q v_v + (1 - x_q)v_l$ (m <sup>3</sup> /kg)]
$Nu$	local Nusselt number based on $D_h$	<b>Subscripts</b>	
$\dot{m}$	mass flow rate (kg/s)	c	critical condition
$M_w$	molar mass (g/mol)	f	water
$P$	local fluid pressure (Pa)	l	liquid
$p$	wetted perimeter (m)	p	prediction
$Pr$	liquid refrigerant Prandtl number, $c_p \mu / k _{r,l}$	r	refrigerant
$q''$	local heat flux based on $A_i$ (W/m <sup>2</sup> )	s	saturated state
$Re$	all liquid, refrigerant Reynolds number based on $D_h$ , $Re = G_r D_h / \mu_{r,l}$	v	vapor
$s$	distance between fins (mm)	w	heat transfer surface

nenbau GmbH, 2012). Consequently, flow boiling heat-transfer data for micro-fin tubes with R1234yf/R134a (56/44) and R1234ze(E) are essential for the evaluation of their use in unitary applications.

Much of the relatively recent research on flow boiling in micro-fin tubes has been done on traditional refrigerants. For example, Targanski and Cieslinski (2007) and Hu et al. (2011) measured the evaporation heat-transfer characteristics of R407C and R410A, respectively, inside a micro-fin tube in the presence of oil. Zhang et al. (2007) measured the evaporation heat-transfer coefficients of R417A and R22 inside a micro-fin tube and introduced a new heat-transfer correlation to predict their values. Muzzio et al. (1998) and Chamra and Webb (1995) investigated the heat-transfer performance of micro-fin tubes with R22. Yun et al. (2002) examined existing experimental data and developed a model, which was validated for use with R22, R113, R123, R134a, and R410A, and a variety of micro-fin tube geometries. Seo and Kim

(2000), Yu et al. (2002), and Kim et al. (2002) measured the flow boiling heat-transfer coefficient in micro-fin tubes for R22, R134a, and R410A, respectively. Well-sandt and Vamling (2005) investigated in-tube evaporation of R134a in a special type of micro-fin tube where the fin rifling, instead of being continuous, was arranged into V-grooves that resembled herringbones; hence, it is called the herringbone micro-fin tube. Oliver et al. (2004) also studied the two-phase heat-transfer performance of a herringbone and a standard 18-deg helical micro-fin tube with R22, R134a, and R407C.

Because of the relatively recent introduction of R1234yf/R134a (56/44) and R1234ze(E), measured heat-transfer data in a micro-fin tube are not available in the literature for these refrigerants. The flow boiling measurements that presently exist for R1234ze(E), as in Grauso et al. (2013) and Hossain et al. (2013), are for horizontal smooth tubes. One of the few recent works with R1234ze(E) in micro-fin tubes was conducted by Koyama

et al. (2011); however, this was a condensation study. Presently, there are no flow boiling measurements for R1234yf/R134a (56/44) in a micro-fin tube. Consequently, the present study provides measured local flow boiling heat transfer for two low-GWP refrigerants [R1234yf/R134a (56/44), and R1234ze(E)] and R134a in a micro-fin tube.

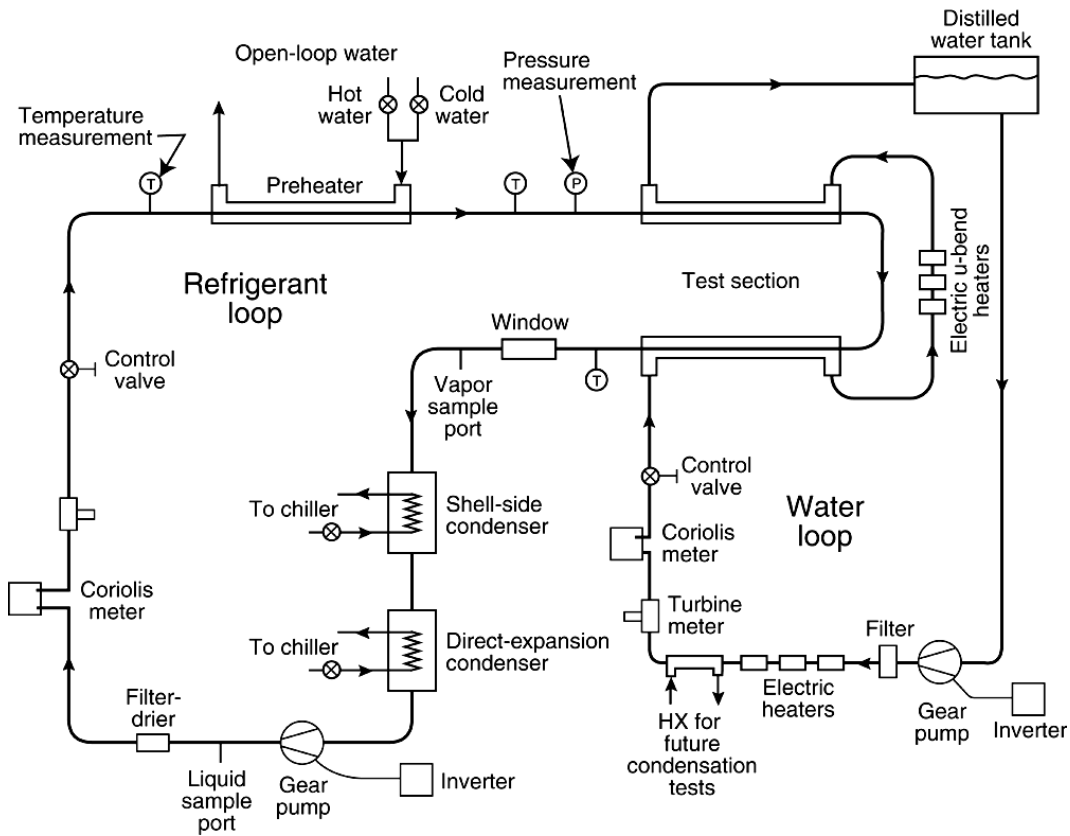
**2. EXPERIMENTAL APPARATUS**

Figure 1 shows a sketch of the experimental apparatus used to establish and measure the convective boiling. The experimental test facility consisted of two main systems: the refrigerant loop and the water loop. The refrigerant flow rate, pressure, and superheat were fixed at the inlet to the test section. The water flow rate and the inlet temperature were fixed to establish the overall refrigerant quality change in the test section. The water temperature drop, tube wall temperature, refrigerant temperatures, pressures, and pressure drops were measured at

several axial locations along the test section. These measurements were used to calculate the local heat-transfer coefficient for the micro-fin tube.

The test section consisted of a pair of 3.34-m-long, horizontal tubes connected by a U-bend. A fixed test pressure was maintained by balancing the refrigerant duty between the subcooler, test section, and evaporator. A magnetically coupled gear pump delivered the test refrigerant to the entrance of the test section with a few degrees of vapor superheat. Another magnetically coupled gear pump supplied a steady flow of water to the annulus of the test section. The inlet temperature of the water loop was held constant for each test with a water-chilled heat exchanger and variable electric heaters. The refrigerant and water flow rates were controlled by varying the pump speeds using frequency inverters. Redundant flow rate measurements were made with coriolis and turbine flowmeters for both the refrigerant and water sides.

Figure 2 shows a cross section of the test section with detail of the micro-fin tube geometry. The test refrigerant



**FIG. 1:** Schematic of the test rig.

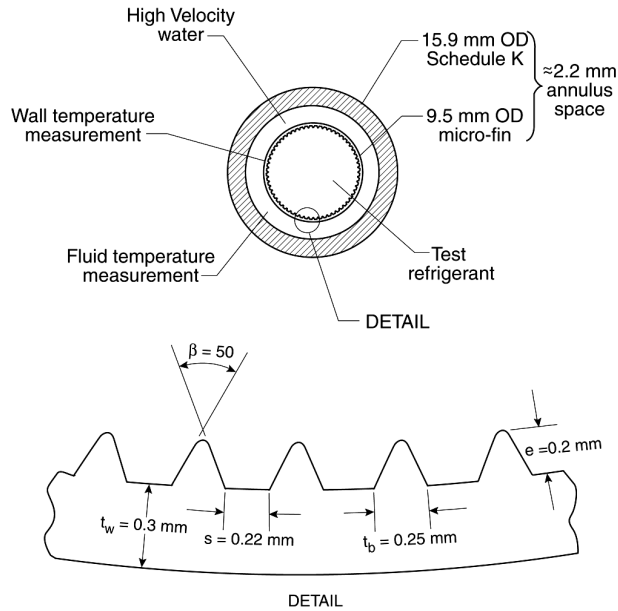


FIG. 2: Test section cross section.

ant flowed inside the micro-fin tube, while distilled water flowed either in parallel flow or counterflow to the refrig-

erant in the annulus that surrounded the micro-fin tube. Having some tests in parallel flow and others in counterflow produced a broad range of heat fluxes at both low- and high-flow qualities. The annulus gap was 2.2 mm, and the micro-fin tube wall thickness was 0.3 mm. The micro-fin tube had 60 fins (0.2 mm high) with an 18° helix angle. For this geometry, the cross-sectional flow area was 60.8 mm<sup>2</sup>, giving an equivalent smooth diameter ( $D_e$ ) of 8.8 mm. The root diameter of the micro-fin tube was 8.91 mm. The inside-surface area per unit length of the tube was estimated to be 44.6 mm. The hydraulic diameter ( $D_h$ ) was measured with a polar planimeter from a scaled drawing of the tube cross section and was determined to be approximately 5.45 mm. The ratio of the inner surface area of the micro-fin tube to the surface area of the smooth tube of the same  $D_e$  was 1.6. The fins rifled down the axis of the tube at a helix angle of 18° with respect to the tube axis.

Figure 3 provides a detailed description of the test section. The annulus was constructed by connecting a series of tubes with 14 pairs of stainless steel flanges. This construction permitted the measurement of both the outer micro-fin wall temperature and the water temperature drop, as will be discussed in the following two paragraphs. The design also avoided abrupt discontinuities

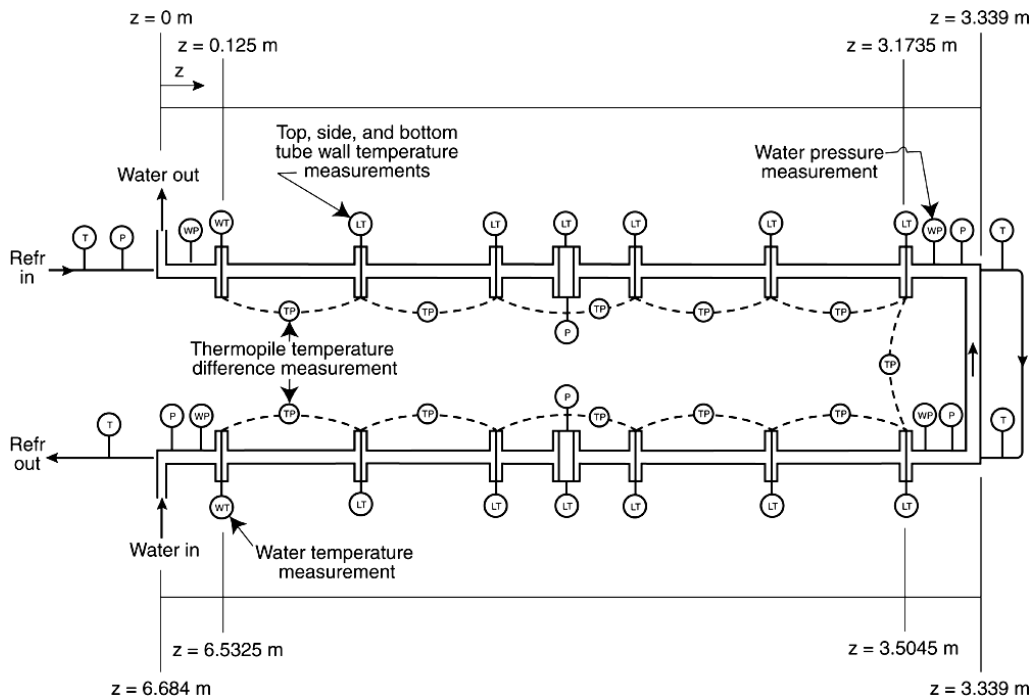


FIG. 3: Detailed schematic of the test section.

such as unheated portions of the test section and tube-wall fins between thermopile ends.

Figure 3 shows that thermocouple wires pass between 12 of the gasketed flange pairs to measure the refrigerant tube wall temperature at 10 locations on the top, side, and bottom of the tube wall. On average, these locations were separated by 0.6 m and were located near the intersection of the shell flanges. In addition to these, thermocouples were also mounted next to the pressure taps near the middle of each test section length. The thermocouple junction was soldered to the outside surface and was sanded to a thickness of 0.5 mm. The leads were strapped to a thin non electrically conducting epoxy layer on the wall for a distance of 14.3 mm before they passed between a pair of shell flanges. The wall temperature was corrected for a heat flux-dependent fin effect. The correction was typically 0.05 K. Figure 3 also shows that a chain of thermopiles was used to measure the water temperature drop between each flange location. Each thermopile consisted of 10 thermocouples in series, with the 10 junctions at each end evenly spaced around the circumference of the annulus. Because the upstream junctions of one thermopile and the downstream junctions of another enter the annulus at the same axial location (except at the water inlet and outlet), the junctions of the adjacent piles were

alternated around the circumference. A series of Teflon half rings attached to the inner refrigerant tube centered the tube in the annulus. The half rings were circumferentially baffled to mix the water flow. Mixing was further ensured by a high water Reynolds number (Kattan et al., 1995).

As shown in Fig. 3, the six refrigerant pressure taps along the test section allowed measurement of the upstream absolute pressure and five pressure drops along the test section. Two sets of two water pressure taps were used to measure the water pressure drop along each tube. Also, a sheathed thermocouple measured the refrigerant temperature at each end of the two refrigerant tubes, with the junction of each centered radially. Only the thermocouple at the inlet of the first tube was used in the calculations. The entire test section was wrapped with 5 cm of foam insulation to minimize heat transfer between the water and the ambient.

### 3. MEASUREMENTS

Table 1 shows the expanded measurement uncertainty ( $U$ ) of the various measurements along with the range of each parameter in this study. The  $U$  was estimated with the law of propagation of uncertainty. All expanded measurement

**TABLE 1:** Median estimated 95% relative expanded uncertainties for measurements ( $U$ )

Parameter	Minimum	Maximum	$U$ (%)
$G_r$ (kg/m <sup>2</sup> · s)	100	418	2.0
$T_s$ (K)	293.0	323.0	0.1 (0.3 K)
$P$ (kPa)	270	450	1.5
$T_w$ (K)	279.0	293.0	0.1 (0.25 K)
$\dot{m}$ (kg/s)	0.010	0.030	2.0
$T_f$ (K)	281.0	321.0	0.1
$P_f$ (kPa)	200	110	1.0
$q''$ (kW/m <sup>2</sup> )	2.6	42.2	5.1
$dT_f/dz$ (K/m)	0.016	0.43	5.2
Nu	112	460	16.4
Re	2191	10800	4.0
Bo	0.000037	0.00063	16.0
$P_r$	3.6	4.2	2.0
$P_s/P_c$	0.06	0.12	2.0
$x_q$	0.003	0.82	8.0
$\Delta T_s$ (K)	1.3	7.6	15.2 (0.44 K)

uncertainties are reported at the 95% confidence level following the NIST guidelines detailed by Taylor and Kuyatt (1994). The estimates shown in Table 1 are median values of  $U$  for the correlated data. Saturated refrigerant properties were evaluated at the measured saturation pressure with the *REFPROP* (Lemmon et al., 2010) equation of state, with the exception of the saturated temperature ( $T_s$ ) and pressure ( $P_s$ ) of R1234yf/R134a (56/44), which were directly measured with a constant volume vessel, temperature bath, glass-rod standard platinum resistance thermometer, and pressure transducer. The measured temperature and pressure for R1234yf/R134a (56/44) is presented in Table 2 and correlated below as follows:

$$T_s = 1/[0.00571 - 3.25 \times 10^{-4} \ln P_s - 5.30 \times 10^{-6} (\ln P_s)^2] \quad (1)$$

The uncertainty in the temperature measurement was less than  $\pm 0.01$  K while the uncertainty in the pressure measurement was within  $\pm 1$  kPa.

The convective boiling heat-transfer coefficient based on the actual inner surface area ( $h_{2\phi}$ ) was calculated as

$$h_{2\phi} = \frac{q''}{T_w - T_s} \quad (2)$$

where the measured wall temperatures ( $T_w$ ) were fitted to their axial position to reduce the uncertainty in the measurement.

Figure 4 shows the estimated expanded uncertainty of the wall temperature fit for all the measurements as a function of thermodynamic quality. Figure 4 includes some data that were omitted from the correlation, as explained in the Results section. The uncertainty of roughly 90% of the fitted wall temperatures was less than 0.5 K at the 95% confidence level. The median of the uncertainty in  $T_w$  was approximately 0.3 K (as shown in Table 1).

The water temperature ( $T_f$ ) was determined from the measured temperature change obtained from each thermopile and the inlet water temperature measurement. The water temperature gradient ( $dT_f/dz$ ) was calculated with second-order finite-difference equations using the measured water temperatures and their locations along the tube length,  $z$ . The water temperature gradients were then fitted with a quadratic polynomial with respect to the tube length. As a check on the water temperature gradient calculation, Fig. 5 shows that the measured water temperatures (open circles) typically agreed with the integrated quadratic fit of the water temperature gradient (solid line) to within 0.2 K.

The fitted, local, axial water temperature gradient ( $dT_f/dz$ ), the measured water mass flow rate ( $\dot{m}_f$ ), and the properties of the water were used to calculate the local heat flux ( $q''$ ) to the micro-fin tube based on the actual inner surface area using the first law of thermodynamics:

$$q'' = \frac{\dot{m}_f}{p} \left( c_{pf} \frac{dT_f}{dz} + v_f \frac{dP_f}{dz} \right) \quad (3)$$

where  $p$  is the wetted perimeter of the inside of the micro-fin tube. The specific heat ( $c_{pf}$ ) and the specific volume ( $v_f$ ) of the water were calculated locally as a function of the water temperature. The water pressure gradient ( $dP_f/dz$ ) was linearly interpolated between the pressure taps to the location of the wall thermocouples. The pressure gradient term was typically less than 3% of the temperature gradient term. Figure 6 plots the relative uncertainty of the heat flux measurement versus the thermodynamic quality. As shown in Fig. 6, the uncertainty of the heat flux remains less than 3% of the measured value, while the average uncertainty is approximately 1.5% of the measured value.

Figure 7 shows example plots of the local heat flux as calculated from Eq. (3) versus the thermodynamic quality for both cases when the water and the refrigerant are in counterflow and parallel flow, respectively. Both heat flux profiles are for R134a at an all-liquid Reynolds number ( $Re$ ) of roughly 7000 and a refrigerant reduced pressure of approximately 0.11. The discontinuity exhibited in the heat flux profiles is due to the change in refrigerant saturation temperature caused by the adiabatic pressure drop in the bend that is used to transition from the first leg of the test section to the second leg. The decrease in the refrigerant saturation temperature causes an increase in the difference between the water and the refrigerant temperature, which leads to an increase in the local heat flux. For the counterflow case, the heat flux increases from approximately 3 kW/m<sup>2</sup> at a quality near 0 to approximately 29 kW/m<sup>2</sup> at a quality slightly greater than 0.8. The parallel flow case is nearly the mirror image of that for counterflow, where the heat flux decreases from approximately 30 kW/m<sup>2</sup> at a quality near 0.06 to approximately 3 kW/m<sup>2</sup> at a quality slightly greater than 0.85.

The thermodynamic and transport properties were calculated with *REFPROP* (version 9.0) (Lemmon et al., 2010) while using enthalpy and pressure as inputs. The enthalpy of the refrigerant liquid at the inlet of the test section was calculated from its measured temperature and pressure. The subsequent increase in refrigerant enthalpy along the test section was calculated from the local heat flux and the measured refrigerant mass flow rate. The

**TABLE 2:** Measured saturated temperature and saturated pressure of R1234yf/ R134a (56/44)

$T_s$ (K)	$P_s$ (kPa)								
303.05	809.3	284.44	467.8	274.76	339.9	283.74	457.5	290.03	556.4
302.55	798.8	283.93	460.4	275.08	343.7	283.73	457.5	290.33	561.4
302.06	788.5	283.44	453.2	275.41	347.5	283.74	457.5	290.62	566.4
301.56	778.0	282.94	446.0	275.73	351.4	283.74	457.5	290.91	571.4
301.06	767.6	282.44	438.9	276.05	355.2	283.74	457.5	291.20	576.4
300.58	757.1	281.93	431.8	276.37	359.0	283.73	457.5	291.50	581.5
300.09	746.6	281.43	424.8	276.69	362.9	283.74	457.5	291.79	586.7
299.59	736.3	280.92	417.9	277.01	366.8	283.73	457.5	292.09	591.8
299.10	726.2	280.42	411.1	277.32	370.8	283.74	457.5	292.37	597.0
298.61	716.1	279.90	404.1	277.63	374.7	283.73	457.5	292.66	602.2
298.12	706.2	279.39	397.4	277.94	378.5	283.73	457.5	292.96	607.5
297.63	696.6	278.88	390.8	278.25	382.6	283.73	457.6	293.25	612.8
297.14	686.8	278.36	384.0	278.57	386.6	283.74	457.6	293.54	618.1
296.66	677.2	277.84	377.3	278.89	390.6	283.73	457.5	293.83	623.4
296.18	667.9	277.82	377.1	279.19	394.6	283.73	457.5	294.13	628.9
295.68	658.3	277.14	368.7	279.50	398.6	283.73	457.6	294.42	634.3
295.19	649.0	276.26	358.0	279.81	402.6	283.73	457.6	294.71	639.8
294.71	639.9	275.73	351.6	280.11	406.8	283.83	459.0	295.00	645.2
294.22	630.7	275.19	345.2	280.42	410.9	284.14	463.3	295.29	650.7
293.73	621.9	274.65	338.9	280.73	415.0	284.44	467.8	295.58	656.3
293.25	613.1	274.11	332.6	281.02	419.0	284.74	472.2	295.88	662.0
292.76	604.2	273.55	326.4	281.33	423.3	285.03	476.6	296.18	667.8
292.27	595.6	273.00	320.2	281.64	427.5	285.33	481.0	296.47	673.4
291.79	587.0	272.45	314.1	281.94	431.7	285.62	485.5	296.76	679.0
291.29	578.3	271.88	307.8	282.24	435.9	285.92	490.1	297.05	684.8
290.81	570.0	271.31	301.8	282.54	440.1	286.22	494.7	297.35	690.7
290.33	561.7	270.74	295.8	282.84	444.4	286.51	499.2	297.64	696.6
289.83	553.3	271.13	299.6	283.14	448.8	286.80	503.8	297.93	702.5
289.35	545.1	271.15	299.8	283.44	453.1	287.10	508.4	298.22	708.3
288.86	537.1	271.44	302.9	283.74	457.4	287.39	513.1	298.52	714.3
288.37	529.0	271.76	306.4	283.74	457.4	287.69	517.8	298.81	720.3
287.88	521.1	272.11	310.1	283.74	457.4	287.98	522.5	299.11	726.4
287.39	513.3	272.45	313.7	283.74	457.5	288.27	527.2	299.40	732.4
286.90	505.5	272.79	317.5	283.74	457.5	288.57	532.0	299.69	738.6
286.41	497.9	273.12	321.2	283.74	457.5	288.86	536.9	299.99	744.4
285.92	490.3	273.45	324.9	283.74	457.5	289.16	541.7	300.29	750.3
285.42	482.6	273.78	328.7	283.74	457.5	289.45	546.5	300.58	756.5
284.93	475.3	274.11	332.4	283.74	457.5	289.74	551.4	300.87	763.0
						301.47	775.8	301.17	769.2

refrigerant pressures were measured at six pressure taps along the test section. The pressure was linearly interpolated between the taps. The average refrigerant temperature was varied between 1° and 3°C with approxi-

mately 5 K of subcooling at the test section inlet. The open squares in Fig. 5 show the measured refrigerant temperature for an example test run with R1234yf/R134a (56/44).

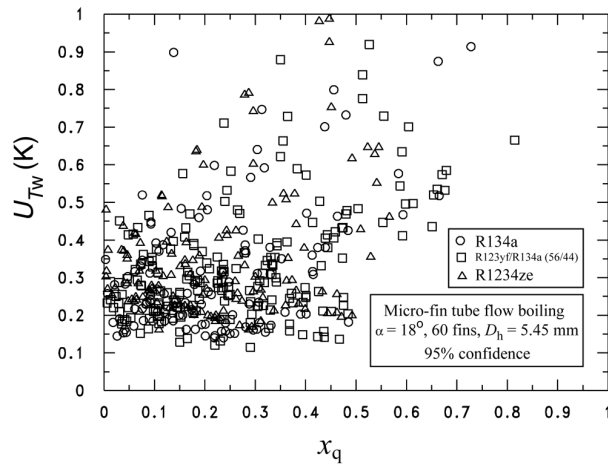


FIG. 4: Relative uncertainty of the inner wall temperature.

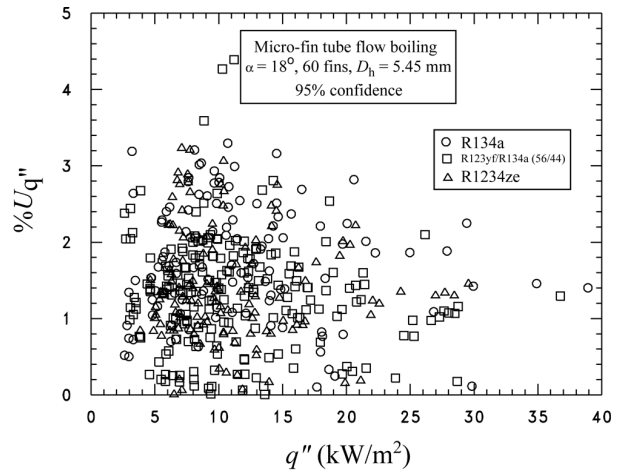


FIG. 6: Relative uncertainty of the water temperature gradient with respect to quality.

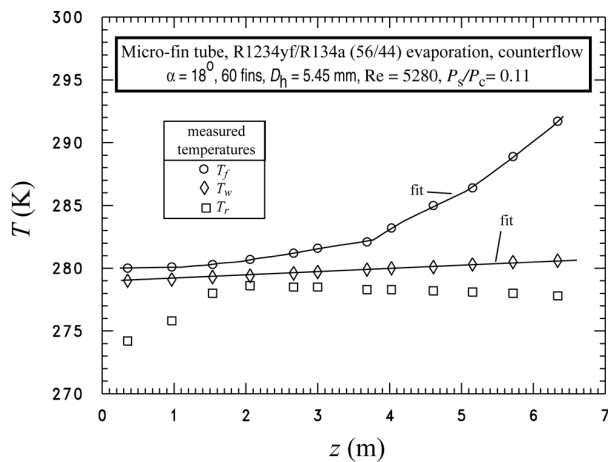


FIG. 5: Counterflow temperature profiles for the R1234yf/ R134a (56/44) test.

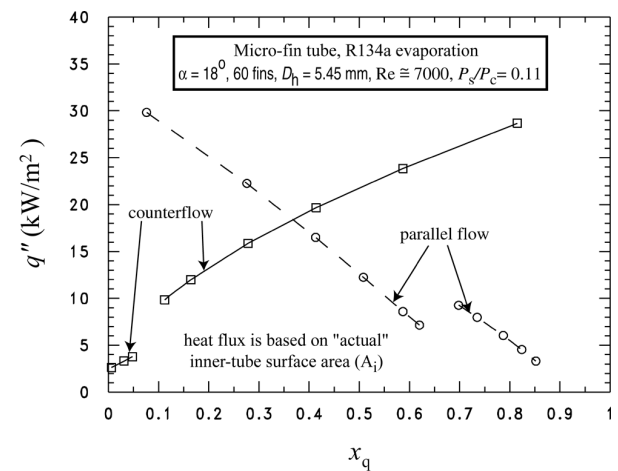


FIG. 7: Heat flux distribution for R134a.

The local Nusselt number (Nu) was calculated using the hydraulic diameter and the heat-transfer coefficient based on the actual inner surface area of the tube as

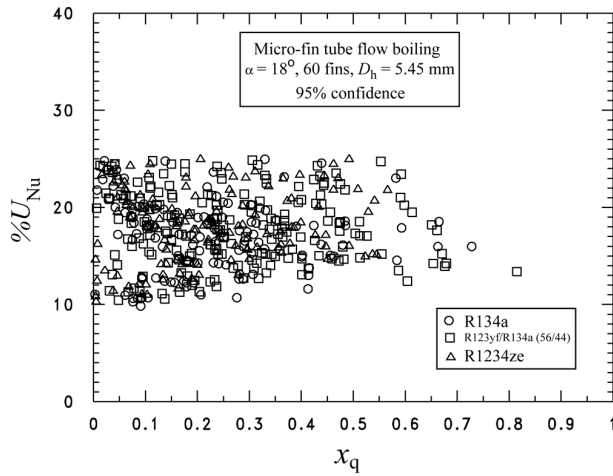
$$Nu = \frac{h_{2\phi} D_h}{k_1} \quad (4)$$

Figure 8 shows that the relative uncertainty of the Nusselt number versus the thermodynamic quality was roughly between 10 and 25%. Measurements of Nu with uncertainties greater than 25% were discarded. The average uncertainty of Nu for the presented data was approximately 18% for all qualities.

#### 4. RESULTS

The 451 data points generated in this study for R134a, R1234yf/R134a (56/44), and R1234ze(E) were tabulated in Kedzierski and Park (2013), which contains the Nusselt and all-liquid Reynolds numbers and other reduced and raw data that are typically used to characterize flow boiling. The raw data measurements, including the heat flux and the wall and water temperatures, are provided for each axial tube location.

The measured local convective boiling Nusselt numbers were compared to the pure-refrigerant (single component) version of the Hamilton et al. (2008) correlation:



**FIG. 8:** Relative uncertainty of the Nusselt number with respect to the quality.

$$Nu = 482.18Re^{0.3}Pr^{C_1} \left(\frac{P_s}{P_c}\right)^{C_2} \times Bo^{C_3} \left(-\log_{10} \frac{P_s}{P_c}\right)^{C_4} M_w^{C_5} \quad (5)$$

where

$$C_1 = 0.51x_q$$

$$C_2 = 0.57x_q - 5.21x_q^2$$

$$C_3 = 0.54 - 1.56x_q + 1.42x_q^2$$

$$C_4 = -0.81 + 12.56x_q - 11.00x_q^2$$

$$C_5 = 0.25 - 0.035x_q^2$$

Here, the all-liquid Reynolds number (Re), boiling number (Bo), liquid Prandtl number (Pr), reduced pressure ( $P_s/P_c$ ), and quality ( $x_q$ ) are all evaluated locally at the saturation temperature. The all-liquid Reynolds and Nusselt numbers are based on the hydraulic diameter ( $D_h$ ). The Nusselt number is also based on the actual inner surface area of the tube. Salient fluid properties (Lemmon

et al., 2010), as they pertain to Eq. (5), are provided in Table 3 for the three test fluids of this study.

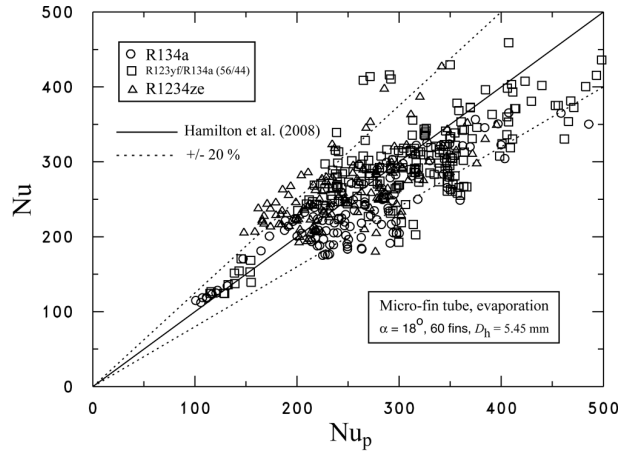
The flow map of Yu et al. (2002) for micro-fin tubes was used to determine that approximately 87% of the measurements were in annular or semi-annular flow. Manwell and Bergles (1990) suggested that the reason annular-like flow is a strong characteristic of micro-fin tubes is that the spiraling fins along the tube axis encourage wetting of the upper tube wall.

Figure 9 shows a comparison between the boiling Nusselt numbers predicted with Eq. (5) for the micro-fin tube to those measured here for R134a, R1234yf/R134a (56/44), and R1234ze(E). Equation (5) predicts 77% of the measured convective boiling Nusselt numbers for R134a, R1234yf/R134a (56/44), and R1234ze in the micro-fin tube to within approximately  $\pm 20\%$ . The measurements for each fluid are roughly centered about the mean of the correlation, suggesting a lack of bias in the prediction due to the different fluids or some other cause. Figure 10 compares the measurements to the Kandlikar and Raykoff (1997) correlation for R134a. Only the R134a fluid-dependent constants were provided by Kandlikar and Raykoff (1997) for prediction. Figure 10 shows that the Kandlikar and Raykoff (1997) correlation overpredicts the measured Nusselt numbers for R134a, on average, by approximately 85%. Because Hamilton et al. (2008) predicted the Nusselt numbers for the new refrigerants well without the need for fluid-specific constants, their results are used in the discussion of Figs. 11–14.

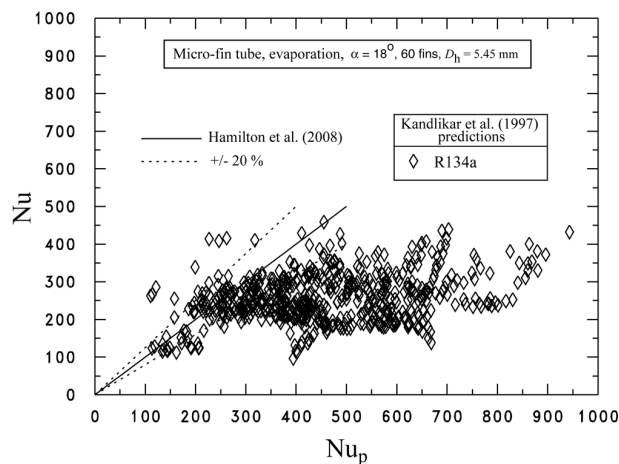
Representative plots of the heat-transfer coefficient ( $h_{2\phi}$ ) versus thermodynamic quality ( $x_q$ ) are given in Figs. 11–14. The solid lines are predictions for the present micro-fin tube geometry, which were obtained from the Hamilton et al. (2008) correlation given in Eq. (5). The symbols are the measured data points, while the dashed lines provide the measurement uncertainty for a 95% confidence level. The uncertainty in the heat-transfer coefficient is shown to be roughly  $1000 \text{ WK}^{-1} \cdot \text{m}^{-2}$  for most of the data for qualities greater than 20%. The uncertainty in the tube wall temperature is the greatest contributor to the uncertainty in the heat-transfer coefficient.

**TABLE 3:** Saturated properties of test fluids at 278 K from REFPROP (Lemmon et al., 2010)

Fluid	$P_s$ (MPa)	$P_c$ (MPa)	$c_{pl}$ (kJ/kg · K)	$i_{tg}$ (kJ/kg)	$k_l$ (W/m · K)	$\mu_l$ (kg/m · s)	$M_w$ (g/mol)
R134a	0.348	4.0593	1.35	194.86	0.090	250.58	102.03
R1234yf/R134a (56/44)	0.415	3.5046	1.33	167.39	0.073	204.72	108.91
R1234ze	0.257	3.6363	1.31	180.96	0.081	253.59	114.04

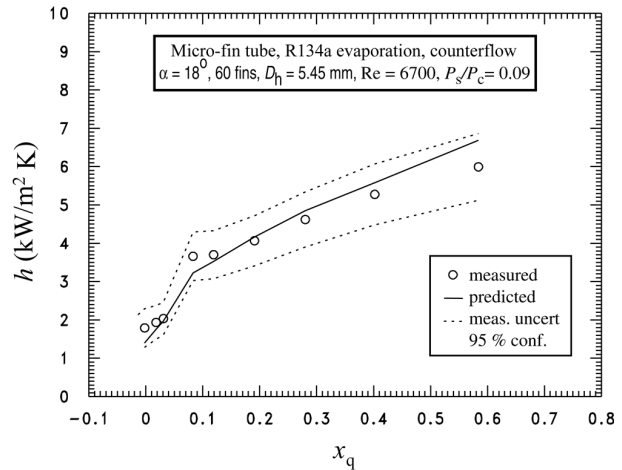


**FIG. 9:** Comparison between the measured Nusselt numbers and those predicted by the Hamilton et al. (2008) correlation.

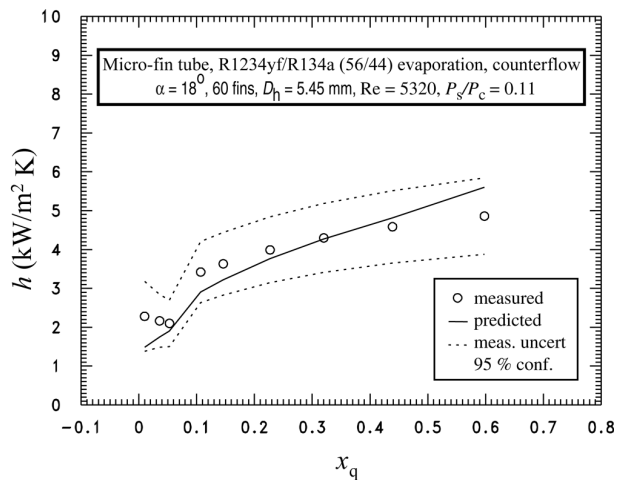


**FIG. 10:** Comparison between the measured Nusselt numbers and those predicted by the Kandlikar and Raykoff (1997) correlation.

Figure 11 shows the local heat-transfer coefficient for R134a for  $Re = 6700$  and  $P_s/P_c = 0.09$  with counterflow between the refrigerant and the water. Half of the measurements are underpredicted by approximately 7.2%, while the other half is overpredicted by approximately 6.2%. Overall, the average difference between the measurements and the predictions is less than 1%. The heat-transfer coefficient increases with respect to quality, in large part, due to the increase of the local heat flux with respect to quality, which is a characteristic of counterflow.



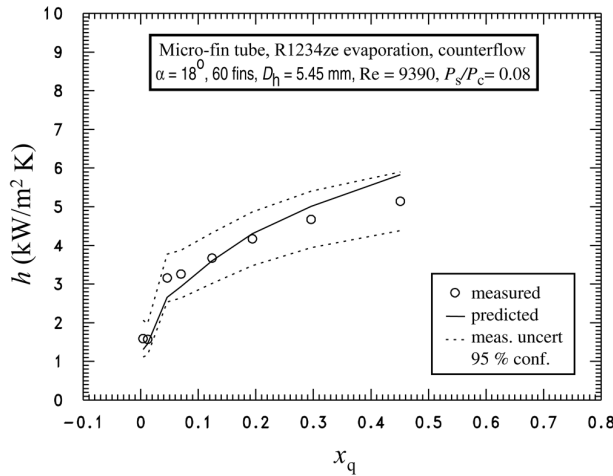
**FIG. 11:** Flow boiling heat-transfer coefficient for the micro-fin tube versus the thermodynamic quality for R134a.



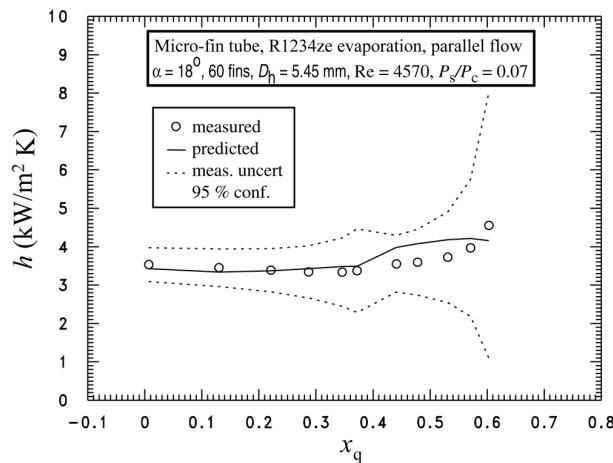
**FIG. 12:** Flow boiling heat-transfer coefficient for the micro-fin tube versus the thermodynamic quality for R1234yf/R134a (56/44).

Figure 12 shows the local heat-transfer coefficient for R1234yf/R134a (56/44) for  $Re = 5320$  and  $P_s/P_c = 0.11$  with counterflow between the refrigerant and the water. For qualities larger than 0.05%, the measurements are predicted to within approximately 10%. Overall, the average difference between the measurements and the predictions is less than 1% for qualities larger than 0.05%.

Figure 13 shows the local heat-transfer coefficient for R1234ze(E) for  $Re = 9390$  and  $P_s/P_c = 0.08$  with coun-



**FIG. 13:** Flow boiling heat-transfer coefficient for the micro-fin tube versus the thermodynamic quality for R1234ze(E) and counter flow.



**FIG. 14:** Flow boiling heat-transfer coefficient for the micro-fin tube versus the thermodynamic quality for R1234ze(E) and parallel flow.

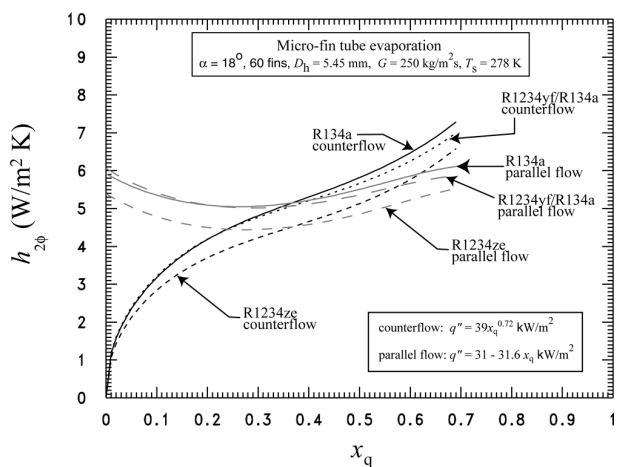
terflow between the refrigerant and the water. Seven of the measurements are overpredicted, on average, by approximately 7.7%, while the remaining four measurements are underpredicted by approximately an average of 12.4%. Overall, the average difference between the measurements and the predictions is less than 1%.

Figure 14 shows the local heat-transfer coefficient for R1234ze(E) for  $Re = 4570$  and  $P_s/P_c = 0.07$ , which presents an example of the parallel flow condition. For qualities larger than 0.05%, half of the measurements

are underpredicted, on average, by approximately 9.2%, while the other half is overpredicted by an average of approximately 7.9%. Overall, the average difference between the measurements and the predictions is less than 1%. For qualities less than 40%, the heat-transfer coefficient decreases with increasing quality. This is mainly caused by the decreasing heat flux with respect to quality, which is a characteristic of parallel flow.

Figure 15 uses the Hamilton et al. (2008) model to illustrate the relative heat-transfer performance of R134a, R1234yf/R134a (56/44), and R1234ze versus quality for the same saturated refrigerant temperature ( $T_s = 278$  K), and the same refrigerant mass flux ( $G_r = 250$   $\text{kg/m}^2 \cdot \text{s}^{-1}$ ) for the present micro-fin tube geometry. Both counterflow and parallel flow conditions are shown. Counterflow is obtained by setting the heat flux to  $q'' = 39x_q^{0.72}$   $\text{kW} \cdot \text{m}^{-2}$ , while parallel flow is obtained for  $q'' = (31 - 21.6x_q)$   $\text{kW} \cdot \text{m}^{-2}$ . The heat flux profiles with respect to quality that were used to calculate the heat-transfer coefficient are approximately equivalent to those shown in Fig. 7. Three different line styles for each flow condition are used to represent the predictions for the three different test fluids as labeled.

In general, for counterflow Fig. 15 shows that the boiling heat-transfer coefficient rapidly increases with increasing quality for qualities less than 20%. For quality ranges between 20 and 70%, the rate of increase in the heat-transfer coefficient with respect to increasing quality is roughly a fourth of that for qualities less than 20%. For the example case presented here, the heat-transfer co-



**FIG. 15:** Flow boiling heat-transfer coefficient for the micro-fin tube versus the thermodynamic quality for R1234ze(E) and parallel flow.

efficient for R1234yf/R134a (56/44) remains within 5% of the heat-transfer coefficient for R134a, having essentially identical performance for qualities less than 30%. For qualities greater than 30%, the heat-transfer coefficient for R1234ze(E) is roughly  $700 \text{ kW/K}^{-1} \cdot \text{m}^{-2}$  less than that of R134a. The smaller heat-transfer coefficient of R1234ze(E) compared to that of R134a is primarily due to the 11% smaller thermal conductivity and the 21% smaller reduced pressure compared to R134a at this test temperature. The justification for this statement can be illustrated by using Eqs. (4) and (5) to calculate the ratio of the heat-transfer coefficient of two fluids (subscripts 1 and 2) at the same mass flux and heat flux and for  $x_q = 0.7$ :

$$\begin{aligned} \frac{h_{2\phi}|_1}{h_{2\phi}|_2} &= \left(\frac{k_{l1}}{k_{l2}}\right)^{0.64} \left(\frac{\mu_{l1}}{\mu_{l2}}\right)^{0.06} \left(\frac{c_{pl1}}{c_{pl2}}\right)^{0.36} \\ &\times \left(\frac{P_s/P_{c1}}{P_s/P_{c2}}\right)^{1.35} \left(\frac{\log_{10} P_s/P_{c1}}{\log_{10} P_s/P_{c2}}\right)^{2.6} \left(\frac{i_{fg}|_2}{i_{fg}|_1}\right)^{0.14} \\ &\times \left(\frac{M_w|_1}{M_w|_2}\right)^{0.23} \end{aligned} \quad (6)$$

Table 4 shows the influence of each the terms in Eq. (6), where fluid 2 [R1234yf/ R134a (56/44) or R1234ze(E)] is referenced to fluid 1, i.e., R134a. The property ratios with the three largest exponents, and consequently the greatest influence for a given percent difference in property, are the liquid thermal conductivity and the reduced pressure. Accordingly, Table 4 shows that the liquid thermal conductivity and the reduced pressure have contributing Eq. (6) terms that differ the most from unity. The larger liquid thermal conductivity and the larger reduced pressure of R134a compared to R1234ze(E) result in a larger heat-transfer coefficient for R134a. Although the larger reduced pressure of R1234yf/R134a (56/44) compared to that of R134a benefits the heat transfer associated with the former, Table 4 shows that the thermal conductivity of R134a is large enough to more than compensate for this effect, resulting in R134a having the

larger heat-transfer coefficient. Consequently, the favorable performance of R134a compared to the low-GWP refrigerants examined here is primarily due to the larger liquid thermal conductivity.

Table 4 also illustrates that for the present comparison the liquid-dynamic viscosity, liquid-specific heat, and latent heat of vaporization all affect the difference in heat transfer compared to R134a by less than 2%. Likewise, the molecular mass has less than a 3% effect on the comparative heat transfer. In addition, Del Col et al. (2002) stated that surface tension effects in the micro-fin tube are negligible for qualities between 0 and 70%. In addition, the surface tension of the three test fluids was essentially the same (approximately 0.011 N/m).

For parallel flow, Fig. 15 shows nearly the same relative and absolute performance for qualities greater than 20%. However, the influence of the larger heat flux is evident for qualities less than 20% for the parallel flow condition. For qualities less than 20%, it is likely that nucleate boiling may be more influential in determining the magnitude of the heat-transfer coefficient than it is for the counterflow condition. In this region, the heat-transfer coefficient is shown to decrease with increasing quality as the nucleate boiling becomes suppressed with the growing presence of annular flow. Otherwise, the heat-transfer coefficient for parallel flow is rather constant with respect to quality varying no more than  $\pm 11\%$  from its mean value over the illustrated quality range.

## 5. CONCLUSIONS

Local convective boiling heat-transfer measurements for two low-GWP refrigerants and R134a in a fluid-heated micro-fin tube were presented. The measured convective boiling Nusselt numbers for all of the test refrigerants were compared to an existing correlation from the literature. Approximately 77% of the measurements were predicted to within  $\pm 20\%$  and centered about the mean prediction.

**TABLE 4:** Relative importance of boiling terms

Fluid	$\left(\frac{k_{l1}}{k_{l2}}\right)^{0.64}$	$\left(\frac{\mu_{l1}}{\mu_{l2}}\right)^{0.06}$	$\left(\frac{c_{pl1}}{c_{pl2}}\right)^{0.36}$	$\left(\frac{P_s/P_{c1}}{P_s/P_{c2}}\right)^{1.35}$ $\times \left(\frac{\log_{10} P_s/P_{c1}}{\log_{10} P_s/P_{c2}}\right)^{2.6}$	$\left(\frac{i_{fg} _2}{i_{fg} _1}\right)^{0.14}$	$\left(\frac{M_w _1}{M_w _2}\right)^{0.23}$
R134a	1	1	1	1	1	1
R1234yf/R134a (56/44)	1.14	1.01	1.00	0.934	0.98	0.99
R1234ze	1.07	1.00	1.01	1.065	0.99	0.97

In general, the measured boiling heat-transfer coefficient increased with increasing qualities for counterflow between the refrigerant and the water. In contrast, for parallel flow, the measured heat-transfer coefficient was relatively constant with respect to quality. The heat-transfer coefficients of the three test fluids were compared at the same heat flux, saturated refrigerant temperature, and refrigerant mass flux by using the correlation from the literature that was validated with the measurements. The resulting comparison showed that refrigerant R134a exhibited the highest heat-transfer performance in large part due to its higher thermal conductivity compared to the tested low-GWP refrigerants. For the example case presented here, the heat-transfer coefficient for R1234yf/R134a (56/44) remained within 5% of the heat-transfer coefficient for R134a, having essentially identical performance for qualities less than 30%. The heat-transfer coefficient for R1234ze(E) was roughly  $700 \text{ kW/K}^{-1} \cdot \text{m}^{-2}$  (approximately 14%) less than that of R134a for qualities greater than 30%. The smaller heat-transfer coefficient of R1234ze compared to that of R134a was primarily due to the 11% smaller thermal conductivity and the 21% smaller reduced pressure compared to R134a at this test temperature.

## ACKNOWLEDGMENTS

This work was funded by NIST. The authors thank Dr. P. Domanski and Dr. A. Persily from NIST, and Dr. D. Han from LACC-JNK, Inc., for their constructive criticism of the first draft of the paper. Thanks also go to Wolverine Tube, Inc., for supplying the Turbo-A, micro-fin tube for the test section, and to Dupont and Honeywell for supplying the R1234yf/R134a (56/44) and R1234ze(E) test refrigerants, respectively.

## REFERENCES

- Bitzer Kuhlmaschinenbau GmbH, Refrigerant Report 17, 2012.
- Chamra, L. M. and Webb, R. L., Condensation and evaporation in micro-fin tubes at equal saturation temperatures, *J. Enhanced Heat Transfer*, vol. **2**, no. 3, pp. 219–229, 1995.
- Del Col, D., Webb, R. L., and Narayanamurthy, R., Heat transfer mechanisms for condensation and vaporization inside a microfin tube, *J. Enhanced Heat Transfer*, vol. **9**, no. 1, pp. 25–37, 2002.
- European Mobile Directive, Directive 2006/40/EC of The European Parliament & of the Council of 17 May 2006 Relating to Emissions from Air-Conditioning Systems in Motor Vehicles & Amending Council Directive 70/156/EC, *Official J. Eur. Union*, vol. **49**, no. L161, pp. 12–18, 2006.
- Grauso, S., Mastrullo, R., Mauro, A. W., Thome, J. R., and Vanoli, G. P., Flow pattern map, heat transfer and pressure drops during evaporation of R1234ze(E) and R134a in a horizontal, circular smooth tube: Experiments and assessment of predictive methods, *Int. J. Refrig.*, vol. **36**, pp. 478–491, 2013.
- Hamilton, L. J., Kedzierski, M. A., and Kaul, M. P., Horizontal convective boiling of pure and mixed refrigerants within a micro-fin tube, *J. Enhanced Heat Transfer*, vol. **15**, no. 3, pp. 211–226, 2008.
- Hickman, K. E., Alternatives to high GWP HFC refrigerants: Chiller applications, *Proc. of ASHRAE/NIST Refrigerants Conference*, Gaithersburg, MD, 2012.
- Hossain, Md. A., Onaka, Y., Afroz, H. M. M., and Miyara, A., Heat transfer during evaporation of R1234ze(E), R32, R410A, and a mixture of R1234ze(E) and R32 inside a horizontal smooth tube, *Int. J. Refrig.*, vol. **36**, pp. 465–477, 2013.
- Hu, H., Ding, G., Huang, X.-C., Deng, B., Gao, Y.-F., Experimental investigation and correlation of two-phase heat transfer of R410A/oil mixture flow boiling in a 5-mm microfin tube, *J. Enhanced Heat Transfer*, vol. **18**, no. 3, pp. 209–220, 2011.
- Intergovernmental Panel on Climate Change (IPCC), Climate Change 2007: The physical science basis—Contribution of Working Group I to the fourth assessment report of the Intergovernmental Panel Climate Change, *Proc. of Intergovernmental Panel on Climate Change of the World Meteorological Organization and the United Nations Environment Programme (UNEP)*, S. S. Solomon, et al., eds., Cambridge, U.K.: Cambridge University Press, 2007.
- Johnson, P. A., Wang, X., and Amrane, K., AHRI low-GWP alternative refrigerant evaluation program, *Proc. of ASHRAE/NIST Refrigerants Conference*, Gaithersburg, MD, 2012.
- Kandlikar, S. G. and T. Raykoff, T., Predicting flow boiling heat transfer of refrigerants in microfin tubes, *J. Enhanced Heat Transfer*, vol. **4**, no. 4, pp. 257–268, 1997.
- Kattan, N., Favret, D., and Thome, J. R., R-502 and Two near-azeotropic alternatives: Part I—In tube flow-boiling tests, *ASHRAE Trans.*, vol. **101**, no. 1, pp. 491–508, 1995.
- Kedzierski, M. A., and Park, K. J., Horizontal convective boiling of R134a, R1234yf/R134a, and R1234ze(E) within a micro-fin tube with extensive measurement and analysis details, *NIST Technical Note 1807*, U.S. Department of Commerce, Washington, DC, 2013.
- Kim, Y., Seo, K., and Chung, J., Evaporation heat transfer characteristics of R-410A in 7 and 9.52 mm smooth/micro-fin tubes, *Int. J. Refrig.*, vol. **25**, pp. 716–730, 2002.
- Koyama, S., Baba, D., and Nakahata, H., Experimental study on

- heat transfer and pressure drop characteristics of pure refrigerant R1234ze(E) condensing in a horizontal micro-fin tube, *Proc. of International Congress of Refrigeration, Prague, Czech Republic*, ID: 306, 2011.
- Kyoto Protocol, *United Nations Framework Convention on Climate Change*, New York: United Nations, 1997.
- Lemmon, E. W., Huber, M. L., and McLinden, M. O., NIST Standard Reference Database 23, Version 9.0 (private communications with McLinden, National Institute of Standards and Technology, Boulder, CO), 2010.
- Manwell, S. P., and Bergles, A. E., Gas-liquid flow patterns in refrigerant-oil mixtures, *ASHRAE Trans.*, vol. **96**, no. 2, pp. 456-464, 1990.
- Montreal Protocol, *Montreal Protocol on Substances that Deplete the Ozone Layer*, New York: United Nations, 1987 (with subsequent amendments).
- Muzzio, A., Niro, A., and Arosio, S., Heat transfer and pressure drop during evaporation and condensation of R22 inside 9.52-mm O.D. microfin tubes of different geometries, *J. Enhanced Heat Transfer*, vol. **5**, no. 1, pp. 39-52, 1998.
- Olivier, J. A., Liebenberg, L., Kedzierski, M. A., and Meyer, J. P., Pressure drop during refrigerant condensation inside horizontal smooth, helical micro-fin, and herringbone micro-fin tubes, *J. Heat Transfer*, vol. **126**, pp. 687-696, 2004.
- Seo, K. and Kim, Y., Evaporation heat transfer and pressure drop of R-22 in 7 and 9.52 mm smooth/micro-fin tubes, *Int. J. Heat Mass Transfer*, vol. **43**, pp. 2869-2882, 2000.
- Targanski, W. and Cieslinski, J. T., Evaporation of R407C/oil mixtures inside corrugated and micro-fin tubes, *Appl. Therm. Eng.*, vol. **27**, no. 13, pp. 2226-2232, 2007.
- Taylor, B. N. and Kuyatt, C. E., Guidelines for evaluating and expressing the uncertainty of NIST measurement results, *NIST Technical Note 1297*, U.S. Department of Commerce, Washington, DC, 1994.
- Webb, R. L. and Kim, N-H., *Principles of Enhanced Heat Transfer*, 2nd Ed., New York: Taylor & Francis, 2005.
- Wellsandt, S. and Vamling, L., Evaporation of R134a in a horizontal herringbone microfin tube: Heat transfer pressure drop, *Int. J. Refrig.*, vol. **28**, pp. 889-900, 2005.
- Yu, M., Lin, T., and Tseng, C., Heat transfer and flow pattern during two-phase flow boiling of R-134a in horizontal smooth and micro-fin tubes, *Int. J. Refrig.*, vol. **25**, pp. 789-798, 2002.
- Yun, R., Kim, Y., Seo, K., and Kim, H., A generalized correlation for evaporation heat transfer of refrigerants in micro-fin tubes, *Int. J. Heat Mass Transfer*, vol. **45**, pp. 2003-2010, 2002.
- Zhang, X., Zhang, X., and Yuan, X., Evaporation heat transfer coefficients of R417a in horizontal smooth and microfin tubes, *Proc. of International Congress of Refrigeration, Beijing*, ICR07-B1-228, 2007.